Journal of Molecular Catalysis A: Chemical 305 (2009) 24–33

Contents lists available at ScienceDirect

Journal of Molecular Catalysis A: Chemical

journal homepage: www.elsevier.com/locate/molcata

Nanoparticles of Fe_2O_3 inserted in SBA-15 silica at micropore mouth level: An experimental evidence of the confinement effect

S. Valange[a,*], R. Palacio[a], A. Charmot[a], J. Barrault[a], A. Louati[b], Z. Gabelica[c,**]

[a] Université de Poitiers, ESIP, CNRS-LACCO, UMR 6503, 40 Av. Recteur Pineau, F-86022 Poitiers, France
[b] LPI-LEA, ENSCMu, 3 rue A. Werner, F-68093 Mulhouse Cedex, France
[c] LPI-GSEC, ENSCMu, 3 Rue A. Werner, F-68093 Mulhouse Cedex, France

ARTICLE INFO

Article history:
Available online 13 March 2009

Keywords:
Confinement effect
Fe_2O_3/SBA-15
Fe_2O_3 nanoparticles
Iron chelate precursors
Cyclic voltammetry

ABSTRACT

Nanometric Fe_2O_3 particles could be inserted inside the internal pore volume of SBA-15 mesoporous silica when Fe(III) chelates (EDTA, gluconate and citrate) were used as impregnating precursors. Fe(III) nitrate preferentially yields 8 nm uniformly sized Fe_2O_3 clusters that selectively plug the SBA-15 channels through a geometric confinement effect. An oxidative degradation of Fe-chelate precursors yielded Fe(III) oxidic particles of various sizes and dispersion, depending on the nature and geometry of chelate anion. Fe(EDTA) precursors specifically generated Fe_2O_3 nanoparticles that selectively migrate towards two types of positions where the silica surface exhibits a high curvature. In samples involving low Fe loadings, Fe_2O_3 particles first creep towards the silica micropore mouths (nests), in which they are readily confined and stabilized. For higher Fe loadings, when most of the micropore nests were filled, oxidic particles eventually settle as a superficial film on the mesopore walls and undergo stabilization onto the surface roughness that can also favors their confinement, as theoretically predicted by Derouane and co-workers. Upon further reduction, as selectively followed by combined cyclic voltammetry and TPR, Fe_2O_3 readily yield FeO nanoslabs that remain even more efficiently confined within their respective nest positions through a further acid–base type stabilization.

1. Introduction

In 1985, Anderson et al. [1] suggested that the strength of van der Waals type bonding of molecules (e.g. water, hydrocarbons...) on solids could be proportional to the curvature of the solid surface (e.g. internal surface in zeolites). Derouane [2] extended this concept by proposing the concept of "nest effect" image, wherein a (basically gaseous) molecule and its direct (basically solid) environment tend reciprocally to optimize their van der Waals interaction. The new concept emphasized that stereochemical, rather than diffusional effects, favor sorbate molecules to reach minimum energy points on the host (zeolite...) surface. The neat result is an increase of the sorption equilibrium constant and, hence, the local concentration of sorbate species, thereby further affecting the overall reaction kinetics. Nest effects not only concerned highly curved intracrystalline volumes in porous materials (zeolites) but also any active site (located on a flat surface) that sterically favors, through its own geometry, the confinement of a sorbate molecule. Alkylation of aromatics, as reported by Ducarme and Védrine [3], was among the first experimental observations to be readily explained by the "nest effect". Derouane et al. [4,5] could further quantify the role of surface curvature of the "nesting concept". For comparable sizes and shapes of the host surface and of the sorbate, these authors could describe the interaction energy between the host (curved) site and the guest molecule by proposing a simple van der Waals model. In short, the van der Waals interactions are amplified by the curvature of the pore walls with which the molecules optimally interact. The physisorption energy experimented by a guest molecule (idealized as a sphere), as it moves along a flat surface towards the pore opening (idealized as a hemispherical crater) indeed showed a very sharp drop as soon as the molecule sinks into the crater. Derouane and co-workers further demonstrated [4–6] that confinement of molecules in pores of near atomic size also affects various diffusional properties of molecules. They therefore proposed the concept of "floating molecule", where the mobility of small molecules increases when an optimal fit between the size and morphology of the sorbate and its close environment is achieved [4]. Among other examples derived from the so-defined confinement effect emerged the concepts of "molecular docking" [8], "molecular traffic control" [6,9,10] or "confinement catalysis" [6,7].

The "nest" and "confinement" effects developed by Derouane et al. for zeolites could be readily extended to mesoporous mate-

* Corresponding author. Tel.: +33 5 49 45 40 48; fax: +33 5 49 45 33 49.
** Corresponding author. Tel.: +33 3 89 33 68 94; fax: +33 3 89 33 68 15.
E-mail addresses: sabine.valange@univ-poitiers.fr (S. Valange), Zelimir.Gabelica@uha.fr (Z. Gabelica).

1381-1169/$ – see front matter © 2009 Elsevier B.V. All rights reserved.
doi:10.1016/j.molcata.2009.03.001

rials by other groups. Such materials currently have mesopores that often present various pore wall "tortuosities" [11] but they can also involve some microporosity when prepared under specific synthetic conditions [12]. Various authors showed that conversions for some reactions, e.g. oligomerizeation of 1-butene [13] or acetalization of cyclohexanone with methanol [14] over mesoporous materials markedly increased when their pore diameters had restricted dimensions. In both examples, the highest activity was found for pore diameters close to 2 nm while it strongly decreased for narrower or for larger pore sizes, thereby discarding diffusion limitations. These findings were better explained by considering geometric and energetic effects based on the confinement model described by Derouane [4,7]. More recent determinations of the sorption energetics (measured through the corresponding heats of adsorption) in the case of isomerization of n-hexane over MCM-41 also suggested that geometric-dependent conditions (confinement effects) dominate over all other factors [15].

Several experimental evidences were reported showing that molecules can be embedded into narrow spaced voids of various matrixes on which they stay simply sorbed without further reaction. In most such cases, the term "confinement" then means the optimal fitting of a particle within a void space (usually channel) of similar dimensions (geometrical fitting), which does not necessarily imply any further energetic stabilization onto some rough surface, either in mesopores or on a more open system. As a typical example, xenon molecules were shown to first fill the very small mesopores of SBA-15 silica, where the strong sorption was explained by considering "sharp confinement effects" [11]. Similarly, dibenzodioxine was found strongly held only when the substrate pore size closely matches its molecular kinetic diameter, as in the case of mordenite or NaY zeolites that exhibit narrow pores, but not on mesoporous silicas in which they simply stay weakly H-bonded to the internal silanols [16]. Yang et al. [17] have prepared Pd nanoparticles that were found located both within the nanometer-sized SBA-15 silica walls and also within the micropores of the bimodal porous silica, where they could survive various oxidation–reduction treatments. Similarly, an effect of nanoscale pore space confinement on Zn particles was reported to occur when the latter were embedded in mesoporous alumina [18]. In that case, this nanoscale confinement was supposed to affect the particle sorption via the overlap of the electronic double layer within the mesopores, creating a surface complexation environment different from that of an unconfined surface.

Many metal oxide nanoparticles could be similarly encapsulated into the straight channels of various mesoporous silica substrates and stabilized through the same geometrical effect. The internal volume is then called "a confined reactor" into which particles should be considered rather as "encapsulated" (within the walls) than "anchored" (onto the rough surface). Typical recent examples deal with various transition metal oxides readily stabilized into SBA-15 channels through a perfect size fitting, after a controlled calcination of the corresponding precursors [19], or of nanosized La_2O_3 inserted within MCM-41 mesopore walls through some "stereoscopic confinement effect of the host channel on the guest" [20]. To our knowledge, no experimental evidence was reported demonstrating that solid (sub)nanoparticles could be stabilized on external surfaces of bulk substrates or on internal pore walls of mesoporous materials through an energetically favored stabilization on the surface roughness.

We have recently developed the preparation and characterization of a series of SBA-15 mesoporous silica-supported iron oxide composite catalysts, by using the so-called chelate route [21]. It was earlier proposed that when chelate-type transition metal-bearing precursors impregnate MCM-41 silica mesopores, a gel-like phase readily forms and favors, upon further drying, an optimal dispersion of the chelate over the substrate surface as a film, thereby preventing further sintering of the resulting metal oxidic particles after thermal degradation of the metal chelate precursor [22]. Our preliminary findings [21,23] on the Fe/silica system has lead to more elaborated conclusions. It was found that iron chelate precursors were first stabilized through hydrogen-type interactions with the superficial silanols of the silica substrate during the drying step of the impregnated composites. This stabilization caused a decrease of the interaction of the chelate anions with their Fe(III) counterions that were readily released and converted into (sub)nanometric Fe_2O_3 particles during the subsequent chelate thermal degradation. Only strong chelates such as Fe(III)-EDTA had yielded sub-nanometric stable and extremely well dispersed Fe_2O_3 particles. Conversely, the pores of the Fe/SBA-15 composite prepared using Fe(III) nitrate were filled with Fe_2O_3 isolated but more bulky particles, their size being limited by the mesopore diameter of the substrate. In a further in depth comparative study of both systems (Fe-chelate versus Fe nitrate) by combined thermal analysis [24], we have proposed a decomposition model in each case and explained why strong Fe(EDTA) chelates readily yield sub-nanometric oxidic particles while about 8 nm agglomerates were systematically generated when non chelating Fe precursors (Fe(III) nitrate) were used. While these latter were probably stabilized through an eventual encapsulation in the mesopores of equivalent diameter by a classical pore size/particle size fitting (geometric confinement), the remarkable thermal stability of the sub-nanometric Fe_2O_3 particles on the internal mesoporous surface is yet to be explained.

The aim of the present contribution is to further compare the role of different Fe precursors (Fe(III) nitrate and three different iron chelates, namely (Fe(III),Na)-EDTA, (Fe(III),NH_4)-citrate and Fe(II)-gluconate) in yielding Fe_2O_3 particles of variable sizes. In particular, we want to bring convincing experimental evidences arguing for a steady stabilization of Fe_2O_3 (sub)nanoparticles readily generated in the case Fe(EDTA)/SBA-15 composites prepared using increasing Fe(EDTA) loadings. More specifically, we wish to question whether their possible confinement within potential nests or traps intentionally generated onto the mesopore internal walls of SBA-15 prepared by selected synthesis recipes, could be the reason for their high dispersion and strong retention. Several complementary techniques, including TEM/EDX, nitrogen sorption isotherms, TPR and cyclic voltammetry were used to evaluate the final textural and redox properties of the calcined Fe/SBA-15 composites.

2. Experimental

2.1. Sample preparation

Pure siliceous mesoporous SBA-15 was prepared using classical literature procedures [25], but by varying the hydrothermal conditions so as to tailor the pore geometry and "tortuosity" of the substrate [12]. The surfactant, Pluronic P123, was dissolved in a mixture of water and HCl at 40 °C. Tetraethylorthosilicate (TEOS) was added to the surfactant solution and the mixture stirred for 24 h. It was then transferred to Teflon bottles and heated at 100 °C for 3 days. The white solid was filtered, washed with distilled water, air-dried and calcined at 550 °C for 8 h under flowing air. Two different batches with very similar properties were prepared (referred to as SBA-15/1 and SBA-15/2) (Table 1).

Dispersed Fe_2O_3 nanoparticles were generated through a TG/DTA-controlled calcination of the SBA-15/1 silica support containing different Fe(II) and Fe(III) chelate precursors, namely (Fe(III),Na)-EDTA, (Fe(III),NH_4)-citrate and Fe(II)-gluconate, as well as Fe(III) nitrate, used for comparison. Before being used as support, the calcined mesoporous silica was preliminary dehydrated into a Schlenck reactor under vacuum at 120 °C during 4 h. The iron

Table 1
Chemical analysis, sorption properties and TPR reduction peaks of various calcined Fe_2O_3/SBA-15 composites.

Precursor or composite	Fe (wt%)	S_{BET} ($m^2\,g^{-1}$)	Vol. micro ($cm^3\,g^{-1}$)	Vol. meso ($cm^3\,g^{-1}$)	First TPR peak (°C)	2nd and 3rd TPR peaks (°C)
SBA-15/1 calc.	–	810	0.081	1.11	–	–
Fe(nitrate)/SBA-15/1	3.8	770	0.077	1.03	407	NI
Fe(gluconate)/SBA-15/1	3.95	673	0.032	0.75	450	NI
Fe(citrate)/SBA-15/1	3.9	620	0.046	0.80	435	NI
Fe(EDTA)/SBA-15/1	3.6	486	>0.005	0.69	551	805, 910
SBA-15/2 calc.	–	789	0.094	1.14	–	–
Fe(EDTA)/SBA-15/2a	1.4	630	0.072	0.89	524	>1000
Fe(EDTA)/SBA-15/2b	2.5	575	0.041	0.86	531	856, >1000
Fe(EDTA)/SBA-15/2c	3.45	505	0.026	0.81	545	833, >900
Fe(EDTA)/SBA-15/2d	4.5	485	>0.01	0.75	553	820, >900

NI: not investigated.

chelate and nitrate precursors were then inserted at room temperature into the calcined anhydrous silica support through incipient wetness impregnation. This technique is based on the addition of a volume of aqueous solution containing the iron precursor equal to (or lower than) the porous volume of the support determined by nitrogen adsorption. The solution concentration was adjusted in each impregnation step so as to correspond to a complete filling of the substrate pore volume and achieve, after two successive impregnations, the final atomic Fe/Si ratios to 0.035, corresponding to about 3.5 wt% Fe (Table 1). The impregnated solids were dried in air for 2 h at 80 °C, then for 12 h at 120 °C, before being activated up to 450 °C under air flow ($10\,L\,h^{-1}\,g^{-1}$) so as to completely decompose the chelate (or nitrate) anions, and generate the corresponding supported Fe(III) oxidic phases. The final composites were referred to as Fe(gluconate)/SBA-15/1, Fe(citrate)/SBA-15/1, Fe(EDTA)/SBA-15/1 and Fe(nitrate)/SBA-15/1 (Table 1).

In another series of experiments, the calcined SBA-15/2 silica was impregnated with more diluted Fe-EDTA solutions in successive steps and four intermediates involving increasing amounts of Fe were isolated and thermally activated as described above. The final composites were referred to as Fe(EDTA)/SBA-15/2a–d, in the order of increasing Fe content (Table 1).

2.2. Physicochemical characterization

Powder XRD patterns of all the calcined Fe_2O_3/SBA-15/1 and -/2 composites were recorded on a Bruker D5005 diffractometer with monochromatized Cu Kα radiation (λ = 1.5418 Å) at 40 kV, 30 mA. Wide angle spectra were scanned at a rate of $0.04^\circ\,s^{-1}$ and with a step size of 3 s from 20° to 70° 2θ. We have also checked at small angles that the 2D hexagonal structure of the silica templates was maintained during all post-synthesis treatment steps (rate of $0.01^\circ\,s^{-1}$ and with a step size of 20 s from 0.75° to 5° 2θ). Bulk chemical analysis for Fe and Si was achieved by ICP. The decomposition sequence for pure Fe salts and for each composite was followed by combined TG–DTA in flowing air, as described and already discussed in depth elsewhere [24]. The surface area and pore size analysis of the composites was carried out by adsorption–desorption of nitrogen on a Micromeritics ASAP 2010 instrument (−196 °C). Prior to N_2 adsorption, the samples were degassed under vacuum at 250 °C for more than 6 h. Nitrogen α_s-plot method was used to evaluate the microporous volume of the composites. A pure Si–MCM-41 prepared in alkylamine media [26] was used as non-microporous reference.

The overall morphology, mesoporous regularity and surface roughness of the Fe_2O_3/SBA-15/1 composites, as well as their iron analysis, were investigated by TEM (Philips CM120 microscope) coupled to an EDX analyzer (fixed probe) for Fe spot detection over the sample surface. Electron microdiffraction patterns were also recorded to identify the structure of the iron-bearing particles, when visible. Samples were at first included in a resin that was cut into sections of 30–50 nm with a microtome equipped with a diamond cutter, before dispersion on a carbon-coated gold grid. H_2-TPR measurements were performed on all the calcined Fe/SBA-15/1 and -/2 composites pre-treated in argon at 450 °C for 1 h (heating rate of $10\,^\circ C\,min^{-1}$) prior to heating under H_2 flow (5% vol. in Ar) from 20 to 1000 °C at a heating rate of $5\,^\circ C\,min^{-1}$. H_2 consumption was continuously monitored by a thermal conductivity detector.

Voltammetric experiments were performed on a PGSTAT302 Autolab Hardware modulated by Autolab 4.9 software using modified carbon paste electrodes. All measurements were carried out at ambient temperature with a conventional three electrodes configuration, consisting of a platinum wire as auxiliary electrode, a modified sample-paste carbon as working electrode, and a saturated calomel reference electrode (SCE). Pure water (18 MΩ cm, Millipore Milli-Qplus) was used throughout. Potassium chloride (Fluka, Puriss p.a.) was used as supporting electrolyte. The working electrode was constructed by using the following homemade procedure: the main part of the carbon paste electrode, consisting of a Teflon rod (of 1 cm external diameter) filled with the carbon paste and a glassy carbon rod (of 3 mm diameter), was inserted into the other end of the electrode to make the electrical contact. The modified sample-paraffin oil-carbon powder paste was prepared by thoroughly admixing in a mortar the desired amount of sample (typically 20–25 mg) with respectively 55–60 mg of carbon. Paraffin oil ($35–40 \times 10^{-3}$ μL) was then added until a homogeneous paste was obtained. The paste was packed into the electrode and a fresh surface was rapidly generated through rolling out a small plug of the paste with the glassy carbon rod. The plug was subsequently scrapped off and smoothed with a piece of white paper so as to obtain a homogeneous and uniform electrode surface.

3. Results and discussion

3.1. Porosity and pore connections in SBA-15

Galarneau et al. [27] have recently studied in detail the influence of synthesis conditions, more specifically of the hydrothermal temperature, on the variations of the pore system of SBA-15. When the syntheses were run below 80 °C, ultramicroporous silica walls are generated, resulting from the silica templating by the polyethylene oxide 'fingers", forming a corona around each micelle. The resulting mesopores then appear pitted with small ultramicroporous holes that very likely do not bridge the parallel mesopores (Fig. 1A). Around 100 °C, besides a gradual increase of the mesopore diameter and the parallel decrease of the wall thickness, the ultramicroporous pits markedly decrease (in number and possibly ion size) while new secondary micropores start to form and to bridge the parallel mesopores (Fig. 1B). Their diameter is variable and spans between about 1.5 nm (supermicropores) and 4 nm (small mesopores), possibly increasing as a function of synthesis time. The final stage of the pore system evolution is reached

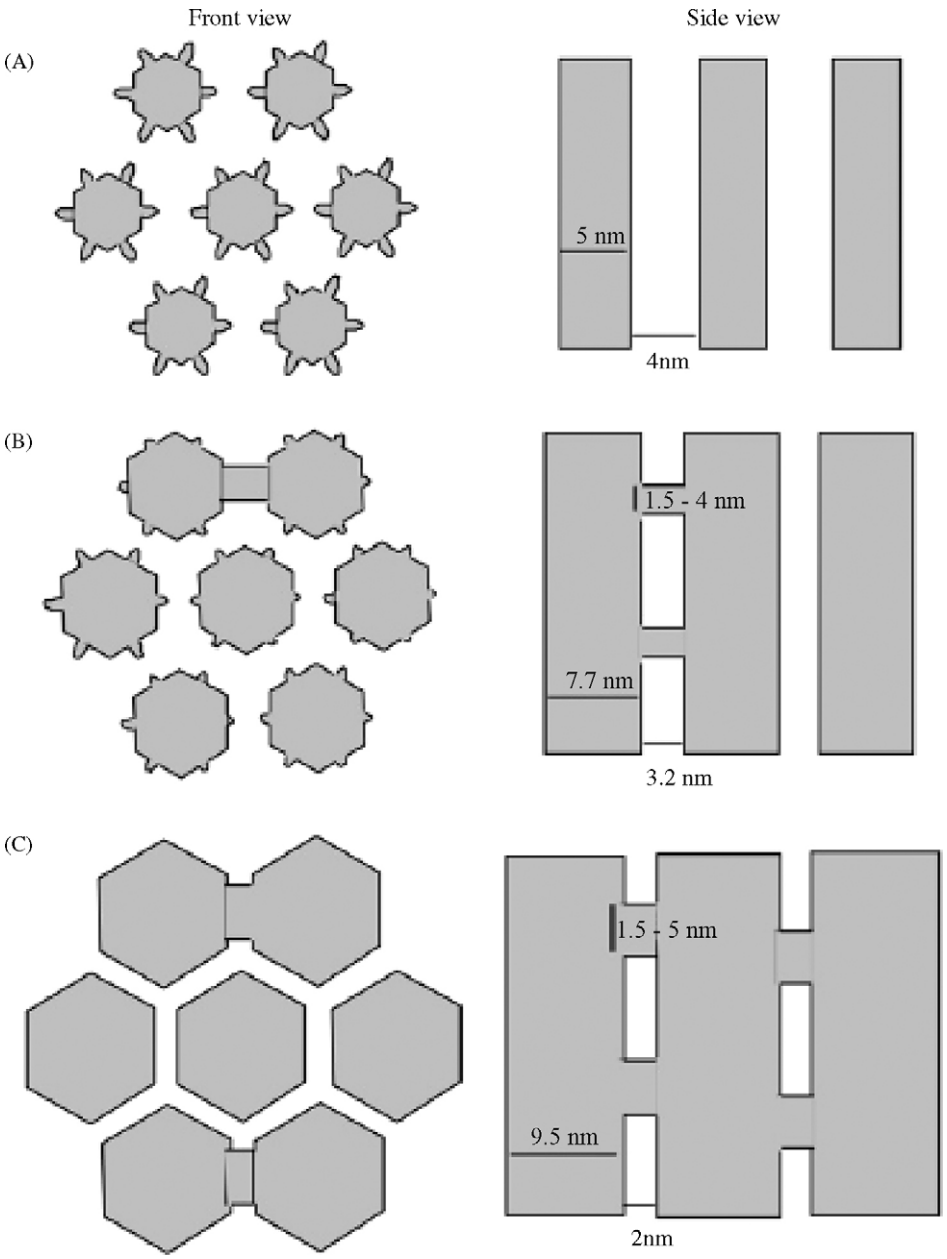

Fig. 1. Schematic representation of SBA-15 synthesis as a function of hydrothermal temperature. (a) Synthesis run below 80 °C showing ultramicroporous pits that do not interconnect parallel mesopores; (b) around 100 °C, micropores of variable diameter start to connect parallel mesopores; (c) at 130 °C larger micropores still interconnect parallel mesopores. (Reproduced from Ref. [27], with permission.)

when the synthesis temperature is adjusted at 130 °C. All ultramicroporosity then disappears while the micropore diameter still slightly increases so that the whole system can be considered as almost completely mesoporous with numerous interconnections (Fig. 1C).

The aim of this contribution being to favor the nanoparticle confinement onto the surface roughness or within the pore mouths of interconnecting micropores, the hydrothermal syntheses of our SBA-15 precursors have been run at 100 °C for 3 days. The extended synthesis time (3 days instead of 1 day as described in [27]) was supposed not to directly affect microporosity but only possibly increase the mesopore wall smoothness by decreasing the number and size of the ultramicroporous pits while the microporosity would still be maintained, so as to favor a more uniform particle dispersion (and size) when they are entrapped into the micropore mouths.

3.2. Structure, morphology and iron loading of Fe/SBA-15 composites

X-ray diffractograms at low angles (spectra not shown but discussed in [21]) confirmed that the hexagonal ordering in the SBA-15 silica was retained after the impregnation/calcinations steps of each composite. At wide angles, the sample synthesized with iron nitrate displayed intense, well-resolved α-Fe_2O_3 XRD lines (confirmed by electron diffraction), indicating that relatively large particles were present. Conversely, no discernable iron oxide reflections were neither visible on the diffractograms of the three calcined composites prepared using chelate complexes, nor for most of the Fe(EDTA)/SBA-15/2 samples with increasing Fe loadings, suggesting the exclusive presence of very small nanometric iron oxide particles (or oxide films) that cause the classical XRD line broadening. Small XRD diffraction lines corresponding to α-Fe_2O_3

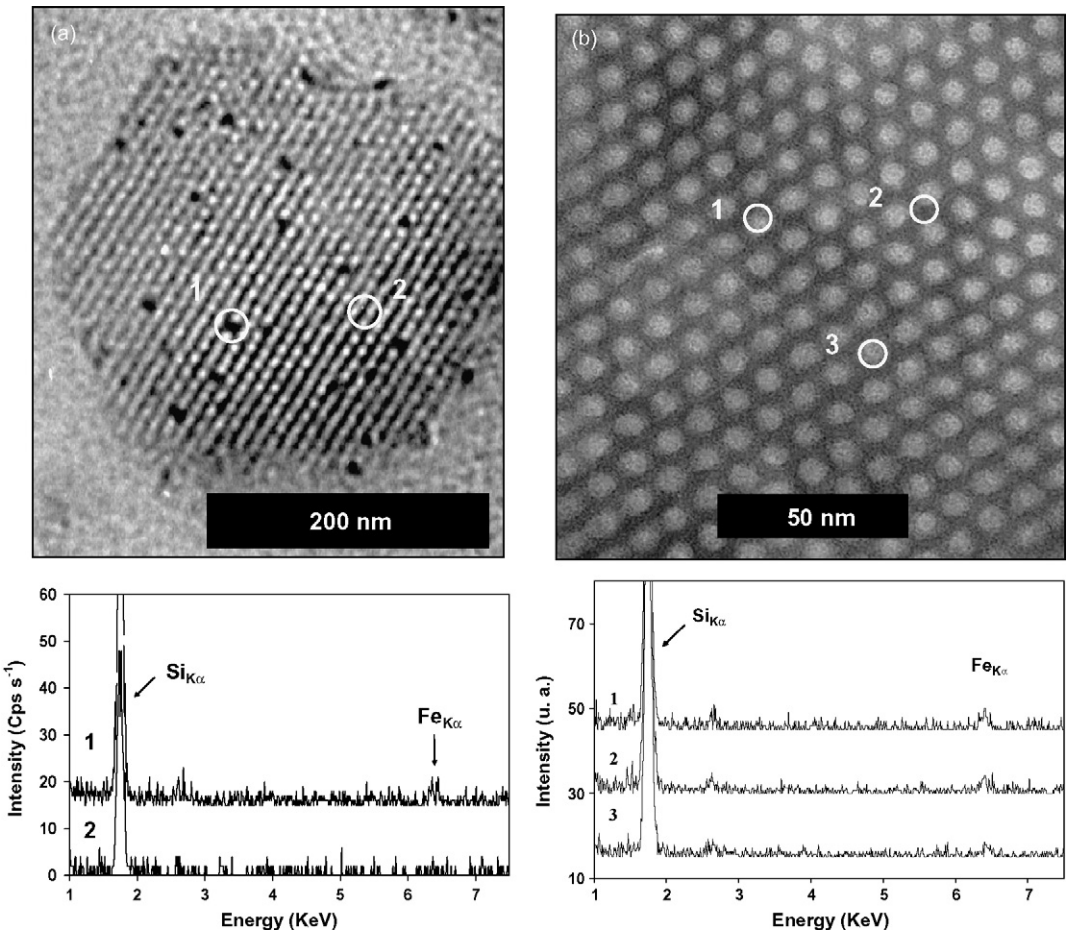

Fig. 2. TEM images of (a) Fe(nitrate)/SBA-15/1 and of (b) Fe(EDTA)/SBA-15/1 composites and the corresponding EDX spot analyses of selected areas, as numbered on the TEM images.

start to appear only for sample Fe(EDTA)/SBA-15/2d (highest Fe loading).

TEM images revealed that the mesopores of the Fe(nitrate)/SBA-15/1 composite were filled with isolated, almost spherical particles. As detailed previously [24], the thermal decomposition of the nitrate precursor results in a fast generation of Fe_2O_3 grains which migrate through the SBA-15 channels during the evaporation of the last solvent traces, resulting in agglomerates of which the size is limited by the silica mesopore diameter (about 8 nm). Each mesopore was shown to be plugged by one Fe_2O_3 particle on average (Fig. 2a). EDX spot analyses of selected empty parts of the mesopores never detected traces of Fe (Fig. 2a), confirming the absence of any surface-confined particles like in the chelate case (see below). This behavior perfectly illustrates the classical case of a geometric confinement of particles encapsulated between the mesoporous walls, as currently observed for various oxidic particles inserted in porous materials. By impeding an eventual growth of the Fe_2O_3 particles, the SBA-15 mesopores also retain them relatively strongly confined because of the optimal contact between the particle and wall surfaces.

In contrast, in the case of Fe(gluconate)/SBA-15/1 composite, spot EDX analyses had confirmed the presence of very small Fe_2O_3 particles homogeneously dispersed throughout the mesopores but hardly visible under TEM conditions ([21], figure not shown). Such particles were even smaller (<2.5 nm) for the Fe(citrate)/SBA-15/1 composite, suggesting an increased chelating efficiency of the citrate anion, compared to that of the gluconate, as elegantly confirmed by combined TG–DTA data [24].

This trend was even more pronounced when EDTA was used as iron complexing agent. In that case indeed, while iron oxide particles could never be visualized by TEM, EDX analyses do detect the presence of iron everywhere throughout the silica matrix, but exclusively inside the mesopores (Fig. 2b). Such species probably consist of a dispersed thin film coating the mesopore walls and involving (sub)nanometric, TEM-silent Fe_2O_3 particles.

The reaction mechanism explaining such coating previously proposed [21,23] and further substantiated by thermoanalytical data [24], can be summarized as follows in the exemplary case of Fe(EDTA)/SBA-15/1 composite. As soon as it is impregnated, the bulky Fe(EDTA) chelate preliminary interacts with the superficial silanol groups of the SBA-15 surface. It is therefore stabilized within the mesopores because it is maintained flat onto the surface through H-bonding. The preliminary stabilization of the chelate anion on the surface and its further steady destabilization and decomposition through heating (under oxidative atmosphere) would soon weaken the coordinative bonds of EDTA with the Fe(III) cations and yield Fe_2O_3. These latter particles stay dispersed because not in contact with each-other, due to their complexation by bulky, flat-lying EDTA, that maintains them separated from each-other. Clearly, the size and dispersion of the Fe_2O_3 particles will depend on the geometry of the chelate anion and its complexing power towards Fe(III); the bulkier the anion, the better its interaction with the surface, the smaller the final Fe_2O_3 particle size.

The next step of this concerted decomposition mechanism concerns the particle stabilization on the silica surface that prevents their steady sintering during subsequent heating. While the Fe_2O_3 particle size could probably be tuned from nanometric to sub-

nanometric dimensions by monitoring the nature (geometry) of the chelate complex used as precursor, their stabilization has not yet been rationally explained. Implication of mesopore surface roughness or of micropore mouths in nanoparticle confining is examined below.

3.3. Localization of confinement sites: surface roughness and micropore probing by nitrogen sorption isotherms

Table 1 lists the pore characteristics of the four Fe/SBA-15/1 composites and of those involving SBA-15/2 precursor impregnated with increasing amounts of Fe(EDTA). For the first series, a significant restriction of the S_{BET} surface area and of the mesoporous and microporous volumes was systematically observed in all iron chelate-impregnated substrates, especially for the sample impregnated with Fe(EDTA). The regular decrease of the mesoporous volume firstly confirmed that Fe_2O_3 particles generated upon degradation of the various chelates were located inside the channels, probably on both sides of the mesopore walls. The fact that, for the chelate-originating composites, the mesoporous volumes were less strongly affected by the insertion of the Fe_2O_3 nanoparticles than the microporous volume, suggests that the oxidic species could have been preferentially deposited inside the silica micropores. Indeed, while the microporous volumes measured in the case of pure SBA-15/1 and for the Fe(nitrate)/SBA-15/1 composite were hardly affected, they almost disappeared in the case of Fe(EDTA)/SBA-15/1 and of Fe(EDTA)/SBA-15/2c and -2d, that involve comparable Fe loadings. Moreover, the initial microporous volume also progressively decreases as a function of Fe loading in samples from the second series, again suggesting that the micropores were preferentially affected by the Fe_2O_3 loading.

It could be reasonably assumed that such very small Fe oxidic species would first migrate towards the silica micropore mouths, thus on positions where the silica surface exhibits a high curvature. The fact that the micropores almost totally disappeared for the composites involving high Fe contents (samples Fe(EDTA)/SBA-15/2c, -2d and sample Fe(EDTA)/SBA-15/1), suggests that Fe_2O_3 particles had plugged (almost) all the micropores. The mean micropore diameter (from 1.5 to 4 nm, Fig. 1) and the relatively wide dispersion of their pore mouths within the mesopores [27], could explain both the small size of the Fe_2O_3 particles and also suggest their strong retention on such sites.

More generally, iron oxide nanoparticles probably start to be first deposited inside the micropores that exhibit the highest curvature for particle confinement (samples Fe(EDTA)/SBA-15/2a and -2b), yielding a population of nanometric isolated and well dispersed particles when EDTA was used as Fe_2O_3 precursor. This does not exclude the presence of iron oxide in other structural configurations for samples with higher Fe contents. One such configuration could possibly correspond to a dispersion of particles along the mesopore surface, as suggested by the decomposition mechanism of the Fe(EDTA) chelate depicted above. Should that surface involve a more pronounced roughness, the retention of such particles would be even stronger.

It appears evident that this confinement (in pore mouths or on a rough surface) would be less marked for samples prepared using Fe(gluconate) and Fe(citrate) complexes, in line with their less pronounced chelating efficiency. Finally, both the microporosity and the mesoporous volume of the parent SBA-15 was hardly affected by the more bulky Fe_2O_3 agglomerates stemming from the nitrate precursor, which is also in line with their strong encapsulation in the mesopores. In short, the more efficient the chelating power of the salt, the best their overcoating of the internal rough surface and/or of the micropore mouths, the smaller the size of the resulting Fe_2O_3 nanoparticles and the stronger their anchoring within the SBA-15 mesophase.

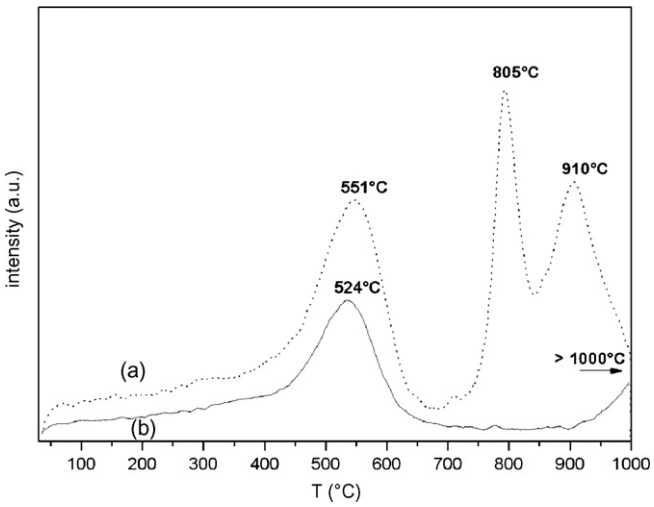

Fig. 3. TPR profiles of (a) sample Fe(EDTA)/SBA-15/1 (3.6% Fe) and of (b) sample Fe(EDTA)/SBA-15/2a (1.4% Fe). Temperatures as indicated.

3.4. Tentative correlation between redox properties (TPR data) and stability of confined Fe_2O_3 particles

3.4.1. TPR data

Temperature-programmed reduction (TPR) was used to probe the ease of Fe(III) to be reduced by flowing hydrogen in our composites. The Fe(III) reducibility being related to the retention strength of the initial Fe_2O_3 nanoparticles, TPR is also expected to further substantiate their confinement.

One first large reduction peak was observed for all the chelate- and nitrate-impregnated solids in the 400–550 °C range. This peak is accompanied by another sharp reduction peak located between about 800 and 850 °C, sometimes followed by another broader peak starting to increase above 900 °C and having its maximum above 1000 °C (except for sample Fe(EDTA)/SBA-15/1 for which it shows a sharp maximum at 910 °C) (Table 1). Fig. 3 shows typical TPR profiles for a Fe-diluted composite (sample Fe(EDTA)/SBA-15/2a and for the same involving more Fe (sample Fe(EDTA)/SBA-15/1).

The quantitative evaluation of H_2 consumption revealed that the first reduction of Fe_2O_3 ended around 700 °C with the formation of FeO in all cases, while the second peak illustrates, sometimes in two steps, the further reduction of FeO to metallic iron. A similar total reduction was also observed in the same temperature range for bulky α-Fe_2O_3 [28] or for Fe_2O_3 inserted in other mesophases such as MCM-41 [29]. This stabilization of FeO can be readily explained by considering that its basic character will favor its anchoring onto the acidic surface of the silica support, preventing its preliminary stabilization as magnetite. The latter compound often appears for unsupported Fe(III) oxides, for example in the case of bulky hematite [28].

In the case of the composite synthesized with iron nitrate, Fe_2O_3 particles of about 8 nm in diameter plugging the SBA-15 channels were reduced at a lower temperature than the probably far smaller particles generated after decomposition of the gluconate, citrate and especially EDTA anions. Several observations however suggest that the temperature variation of the first TPR peak (from about 550 °C for the composites prepared using Fe(EDTA) down to 407 °C for sample prepared with iron nitrate) could be related to the interaction strength of the Fe_2O_3 particles with the support, that in turn (indirectly) depends on their size, assuming that the smallest particles are the most efficiently confined.

Considering the sole particle size, one would have expected the reverse trend, namely that larger particles would have undergone reduction at a higher temperature than the nanometric sized ones,

because of a more restricted hydrogen diffusion towards the core of a bulky slab, as already observed for $CuO–Al_2O_3$ mesoporous composites [30]. This apparent contradiction is easily explained here by considering that the Fe_2O_3 nanoslabs generated through the chelate decomposition are readily confined at the micropore mouths or on the rough mesopore surface so that their contact surface with the support would be predominant when compared to the restricted contact surface of the large 8 nm spheres as in the nitrate composite. Small particles are better confined within the micropore mouths or as tiny films on the mesopore surface roughness and will thus be less readily reached by flowing hydrogen, hence their more difficult reduction.

The higher TPR temperature observed in the case of composites prepared using the chelate route in the second series of samples (Table 1) is also in line with both the particle confinement at the micropore mouths but also with their regular dispersion (in a quasi homogeneous layer) on the silica internal (rough) surface. Indeed, for sample Fe(EDTA)/SBA-15/1 as well as for all the four Fe(EDTA)/SBA-15/2(a–d) samples, the first reduction peak occurs within a restricted temperature range (525–555 °C, Table 1), even for high Fe loadings (sample d). Its intensity is logically proportional to the total amount of Fe in each sample. Although the four Fe(III) → Fe(II) reduction peaks recorded for samples a–d did not appear resolved in two components (that would have corresponded to the two different confined states), these peaks significantly regularly shift towards higher temperatures as a function of Fe loading (from 524 to 551 °C for samples a–d). As particles confined in the micropore mouths are supposed to be predominant in phases involving low Fe amounts (sample a), the above findings suggest that these species undergo reduction at a lower temperature (for example 524 °C, as in sample a) than the particles dispersed as a flat layer onto the pore rough surface, that are more abundant in Fe-richer samples (reduction peak at 551 °C for sample d). The more facile Fe(III) → Fe(II) reduction for nanosized Fe_2O_3 species confined within the micropore mouths, although *a priori* surprising, can be easily rationalized if one considers the acid–base character of both the particle (Fe_2O_3 acidic to amphoteric and FeO basic) and the surface of the substrate (both SiO_2 and SiOH behave as weak acid sites). Because the Fe_2O_3–SiO_2 interaction before reduction is weaker than the FeO–SiO_2 one after reduction, the FeO species that will be the most readily stabilized after reduction would be the best confined one, namely FeO sited in the pore mouths (situation schematically depicted in Fig. 4). As a consequence, its precursor, namely Fe_2O_3 occluded in the same micropore mouths, should then be more readily reduced than its analogue confined onto the mesopore surface.

The second reduction step of the so-generated superficial FeO nanoparticles to metallic Fe is also interesting to consider. This reduction starts around 750–800 °C for all samples except for sample Fe(EDTA)/SBA-15/2a (1.4% Fe), and is visualized by a sharp peak observed between 800 and 850 °C (Table 1). The reduction apparently continues above 900 °C, as suggested by the appearance of a second TPR "bump" above that temperature. Except for sample Fe(EDTA)/SBA-15/1, this second reduction step is not clearly visualized by a sharp peak but rather by a broad baseline increase that was interrupted at 1000 °C (instrumental limitations). H_2 consumptions confirm that the total reduction of Fe(II) to Fe^0 is neither complete after the sharp peak, nor at 1000 °C.

The TPR profile for sample Fe(EDTA)/SBA-15/1 (3.6% Fe) clearly shows that the FeO → Fe^0 reduction occurs in two steps (peaks at 805 and 910 °C) and is almost completely achieved at 1000 °C (Fig. 3A). Conversely, in sample Fe(EDTA)/SBA-15/2a (1.4% Fe), FeO only starts its second reduction above 900°, with no peak maxima recorded at 1000°, while the peak at 800–850 °C is also completely absent (Fig. 3B). It is also interesting to note a regular decrease of the second reduction peak temperature with the Fe loading, for the Fe(EDTA)/SBA-15/2 intermediates (Table 1). These observations are also in line with the presence of two differently confined Fe_2O_3 nanoparticles, thus the one confined at the micropore mouth level (predominant for low Fe loadings), the other probably lying flat as a thin film on the mesopore rough surface (predominant for high Fe loadings). The first species, as soon as reduced into FeO, would be very strongly retained in the pore mouth "funnels" through the above-described acid–base type interaction, presumably stronger than the one characterizing the FeO–SiO_2 interaction in the case of surface-confined species. The first species, supposed to be also more resistant to a further reduction (to Fe^0), would stay stabilized at a higher temperature than the more loosely held FeO particles. As soon as more Fe is loaded, the second FeO species start to predominate (samples Fe(EDTA)/SBA-15/2b to -2d). Although also strongly

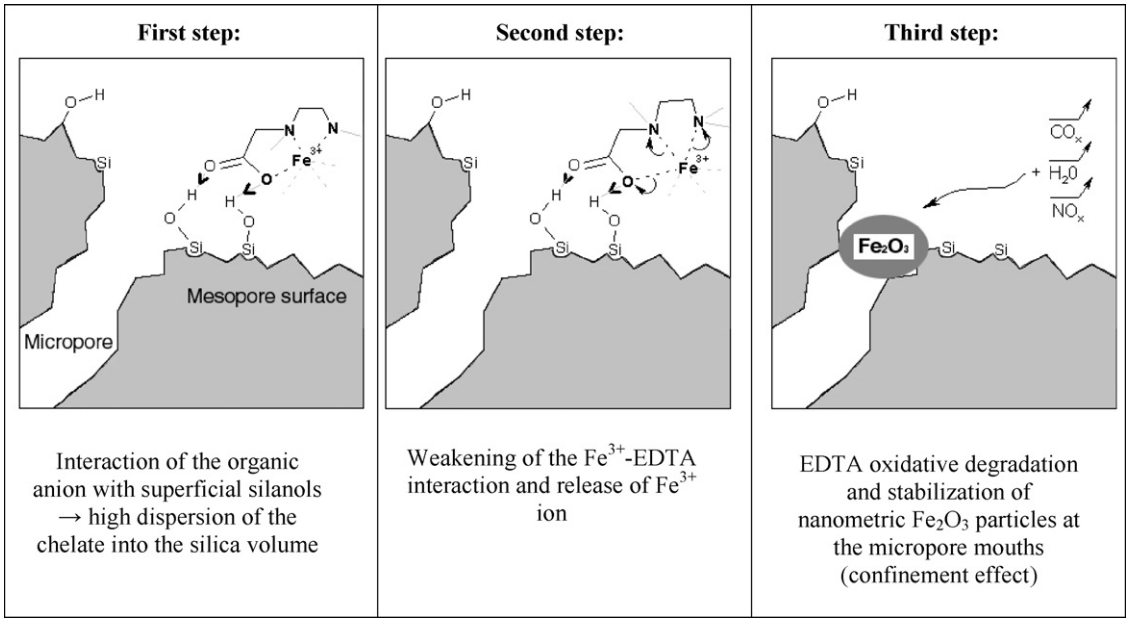

Fig. 4. Mechanism illustrating schematically different steps of the thermal decomposition of Fe(EDTA)/SBA-15 composite, yielding nanosized Fe_2O_3 particles confined at the micropore mouth levels inside the SBA-15 mesopores.

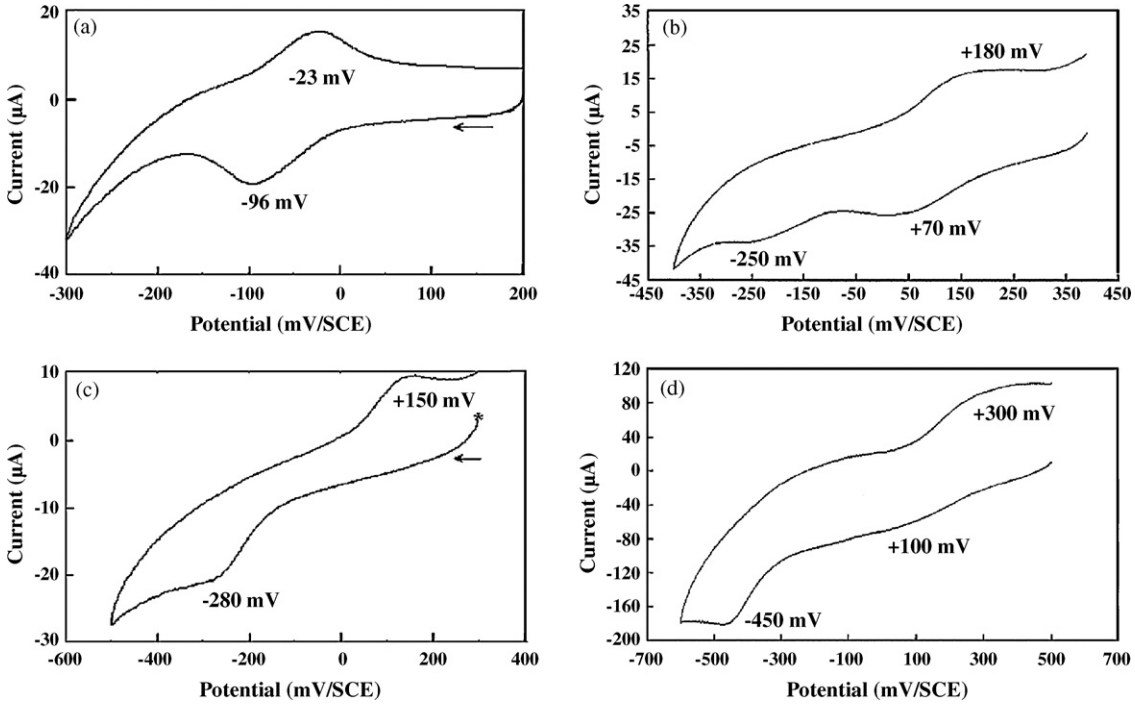

Fig. 5. Cyclic voltammograms of composites: (a) Fe(EDTA)/SBA-15/1; (b) Fe(nitrate)/SBA-15/1; (c) Fe(gluconate)/SBA-15/1; (d) Fe(citrate)/SBA-15/1 recorded with a modified carbon paste electrode in 0.1 M KCl electrolyte with a 25 mV s^{-1} scan rate. Potential values as indicated.

retained on surface, such FeO species probably offer more (external) surface to the flowing hydrogen and are therefore more readily further reduced to Fe^0 than the almost totally hidden particles when deeply embedded into the pore mouth traps with which they are in strong acid–base type interaction.

3.4.2. Cyclic voltammetry (CV)

Fundamentally, cyclic voltammetry is a complementary technique to TPR in terms of detection of the reducing conditions for a species more or less strongly entrapped on a support, provided the diffusion of the reducing agent (flowing hydrogen or electrons through the applied electrode potential) is equivalent. In practice, it is often observed that electrons would more readily reach a reducible electroactive entity than would do hydrogen gas at high temperature, of which the diffusion could be restricted in the case of bulky particles.

In the case of the nitrate-impregnated compound (Fig. 5, curve B), two reduction steps of the initial Fe(III) species were observed (peaks at +70 mV and −250 mV), suggesting either two different Fe(III) bearing species or two consecutive reductions of the same species. Their re-oxidation (Fe(II) → Fe(III)) occurs in one step in the reverse sweep (peak at +180 mV). An evaluation of the number of electrons exchanged per Fe allowed us to attribute the first peak to the reduction of Fe_2O_3 to Fe_3O_4 (1/3 of Fe(III) reduced to Fe(II)), while the second peak at −250 mV most probably reflects the further more difficult reduction of Fe_3O_4 to FeO. A first reduction of Fe(III) to Fe(II) at +70 mV, followed by a further reduction of FeO to Fe^0 was not likely to occur since the re-oxidation peak at +180 mV was not characteristic of a true Fe^0 redissolution phenomenon [31].

In contrast, a more demanding redox process for the other three chelates was observed. In each case, a more difficult reduction of Fe(III) species occurred at a more negative potential than in the nitrate case, thereby indicating that these Fe_2O_3 species interact more strongly with the silica surface. In the case of Fe(gluconate)/SBA-15/1 and Fe(citrate)/SBA-15/1 samples, extended TEM studies had shown that although the SBA-15 surface was found coated with a (probably multilayered) Fe_2O_3 film, an apparent roughness of the coating layer was visible on some places [21]. In Fe(gluconate)/SBA-15/1, some more bulky particles could even be detected (TEM images not shown), in agreement with a less efficient chelating efficiency of gluconate anions towards Fe(III), with respect to citrate.

The $Fe_2O_3 \rightarrow FeO$ reduction potential, respectively −280 mV (gluconate case, Fig. 5, curve C) and −450 mV (citrate case, Fig. 5, curve D), confirms that the Fe_2O_3 generated by using citrate anions is more difficult to reduce electrochemically. Note that while Fe(citrate)/SBA-15/1 is also first partly reduced to magnetite (peak at +100 mV) as in the nitrate case, this intermediate reduction was not detected in the gluconate-bearing sample, for some unknown reason.

The Fe(EDTA)/SBA-15/1 and -/2 samples present very interesting electrochemical characteristics. A first, fully reversible reduction peak appeared at −96 mV when the cyclic voltammogram was recorded at 25 mV s^{-1} scan rate (Fig. 5, curve A). It corresponds to the formation of magnetite, that is readily re-oxidized (peak at −23 mV) when the reduction is stopped at −300 mV and the re-oxidation immediately recorded on the reverse sweep.

The full redox voltammogram of this compound, recorded with a higher scan speed up to −1.2 V, is shown on Fig. 6. While the reversible magnetite formation is now hardly detectable (very broad reduction and oxidation peaks at about −60 and +30 mV respectively), a second peak corresponding to $Fe_3O_4 \rightarrow FeO$ reduction appears at about −710 mV. This far more negative reduction potential, corresponding to a globally demanding reduction, illustrates a better confinement of the Fe(III) species in the EDTA case, if compared to other chelating anions.

Bearing in mind that TPR data suggested that sample Fe(EDTA)/SBA-15/1 involved Fe_2O_3 in two different confined environments, one would have expected to discern also two different reduction peaks in the cyclic voltammogram shown on Fig. 6. We have therefore selected to probe by cyclic voltammetry sample Fe(EDTA)/SBA-15/2b, a compound with intermediate Fe loading (2.5%), assuming both confined species would be present in similar amounts. The voltammogram shown on Fig. 7 indeed very

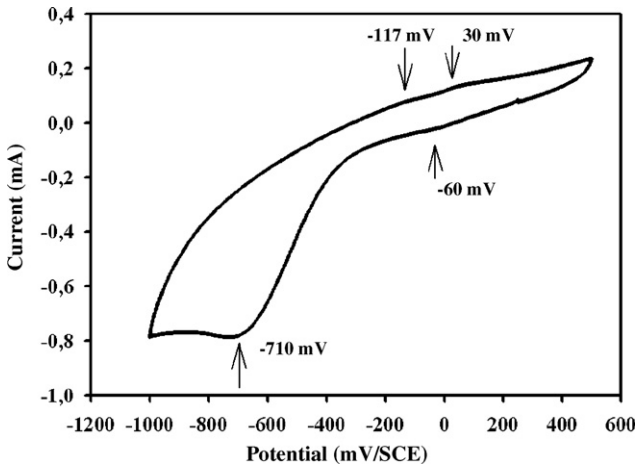

Fig. 6. Cyclic voltammogram of Fe(EDTA)/SBA-15/1 in the more negative potential range, recorded with a modified carbon paste electrode in 0.1 M KCl electrolyte with a 50 mV s^{-1} scan rate. Potential values as indicated.

clearly now shows two reduction peaks (−430 and −780 mV). Their re-oxidation was reversible, as illustrated by the large common "bump" at about −320 mV on the reverse sweep, thereby confirming that both Fe_2O_3 and FeO always remain attached to the substrate internal surface during the redox experiment.

The fact that the reduction occurring at about −710 mV is predominant on the cyclic voltammogram of Fe(EDTA)/SBA-15/1 (3.6% Fe) suggests that the Fe_2O_3 species confined onto the silica rough surface, more abundant than those sited in the pore mouths in that sample, are also more difficult to reduce than the latter. Consequently, the reduction peak that appears at the lower potential (−780 mV) for sample Fe(EDTA)/SBA-15/2b (Fig. 7) should also be attributed to the same surface-confined Fe(III) species, which also fully confirms the TPR conclusions. Similarly, the more facile reduction of the pore mouth-confined Fe_2O_3, visualized by the peak at −430 mV, again confirms the trend of these species to promptly yield very tightly confined FeO particles after reduction. As currently observed in other cases, both species are reversibly re-oxidized on the reverse sweep. The relatively slow electronic exchange between Fe(II) and Fe(III) in this redox process, as illustrated by a medium ΔE value (difference between the main reduction and oxidation peaks) of about 350 mV, remains characteristic of the presence of very small, confined particles [32].

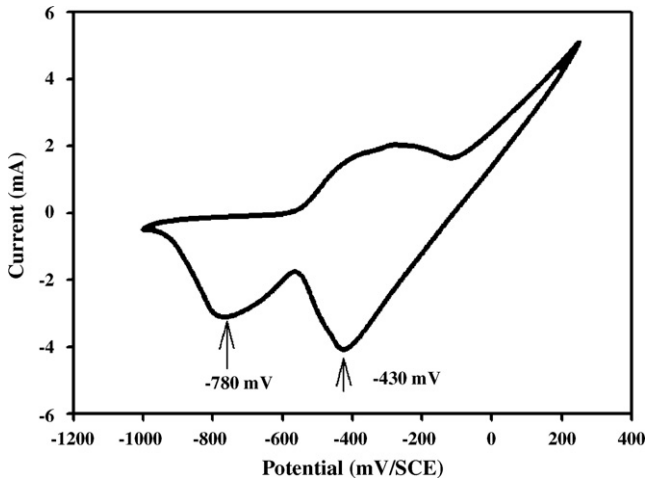

Fig. 7. Cyclic voltammogram of Fe(EDTA)/SBA-15/2b in the more negative potential range, recorded with a modified carbon paste electrode in 0.1 M KCl electrolyte with a 100 mV s^{-1} scan rate. Potential values as indicated.

4. Conclusions

Well dispersed nanometric Fe_2O_3 particles were generated inside the mesopores of SBA-15 silica by incipient wetness impregnation and subsequent calcination of various iron chelates. While the thermal degradation of Fe(III) nitrate precursor yielded large particles encapsulated between the mesoporous walls (classical geometric confinement), Fe(II)-gluconate, Fe(III)-citrate and especially Fe(III)-EDTA complexes generated very small nanometric iron oxide particles inside the mesopores of the silica support. A concerted chelate adsorption/decomposition and Fe_2O_3 release mechanism was proposed to explain both the small oxide particle size and their stabilization on the silica surface that prevents their steady sintering during subsequent heating. A combination of several physico-chemical techniques allowed us to identify two different populations of nanoparticles strongly confined inside the SBA-15 mesoporous walls. Their stabilization occurs through two successive events. In samples involving low Fe loadings, Fe_2O_3 nanoparticles first migrate towards the silica micropore mouths (nests), thus on positions where the silica surface exhibits the highest curvature, in which the particles are readily entrapped and stabilized. This stabilization is schematized on Fig. 4. For higher Fe loadings, when most of the micropore nests were filled, oxidic particles are found eventually deposited as a superficial film and stabilized by the mesoporous surface roughness that can also favor their confinement, as theoretically predicted by Derouane and co-workers [2,4–9]. Upon further reduction selectively followed by cyclic voltammetry and TPR, Fe_2O_3 readily yielded FeO nanograins that stayed even more efficiently confined within their respective nest positions through a further acid–base type stabilization.

The Fe/SBA-15 composites prepared using the chelate route recently proved very promising catalysts for oxidation of phenolic compounds in aqueous media (heterogeneous Fenton catalysis) [21].

Acknowledgments

This work is dedicated to the late Prof. Eric Derouane for his outstanding contribution in initiating and expanding the idea of stabilizing molecules sorbed on substrates through the so-called "confinement effect". He was the first to propose and popularize the concept of "nest effect" and to further generalize its theoretical and practical significance by authoritatively demonstrating its applicability in many domains in physics and chemistry (kinetics, diffusion, floating molecule creeping, confinement catalysis, molecular docking, molecular traffic control. . .). One of us (Z.G.), having had the privilege to work under Eric's skillful guidance for many years, is particularly happy that this original concept could find an elegant experimental application in another domain Eric had thoroughly explored for long years, namely adsorption and stabilization of small metallic particles, potential catalytic active sites, in porous solids.

The authors are also very much indebted to Dr. J. Védrine for his continuous encouragements and support all along this work.

P. Ayrault and F. Moser are sincerely acknowledged for their efficient technical help.

References

[1] S. Anderson, S.T. Hyde, H.G. von Schnerring, Z. Kristallogr. 168 (1984) 1.
[2] E.G. Derouane, J. Catal. 100 (1986) 541.
[3] V. Ducarme, J.C. Védrine, Appl. Catal. 88 (1984) 538.
[4] E.G. Derouane, J.M. André, A.A. Lucas, J. Catal. 110 (1988) 58.
[5] E.G. Derouane, J.M. André, A.A. Lucas, Chem. Phys. Lett. 137 (1987) 336.
[6] E.G. Derouane, Appl. Catal. A 115 (1994) 1.
[7] E.G. Derouane, Appl. Catal. A 134 (1998) 29.
[8] E.G. Derouane, J.B. Nagy, C. Fernandez, Z. Gabelica, E. Laurent, P. Maeljean, Appl. Catal. 110 (1988) 58.

[9] E.G. Derouane, Z. Gabelica, J. Catal. 65 (1980) 486.
[10] N. Dumont, Z. Gabelica, E.G. Derouane, L.B. McCusker, Micropor. Mater. 1 (1993) 149.
[11] A. Nossov, E. Haddad, F. Guenneau, A. Galarneau, F. Di Renzo, F. Fajula, A. Gédéon, J. Chem. Phys. B 107 (2003) 12456.
[12] A. Galarneau, H. Cambon, F. Di Renzo, F. Fajula, Langmuir 17 (2001) 8328.
[13] B. Chiche, E. Sauvage, F. Di Renzo, I.I. Ivanova, F. Fajula, J. Mol. Catal. A 134 (1998) 145.
[14] M. Iwamoto, Y. Tanaka, N. Sawamura, S. Namba, J. Am. Chem. Soc. 125 (2003) 13032.
[15] S. Pariente, P. Trens, F. Fajula, F. Di Renzo, N. Tanchoux, Appl. Catal. A 137 (2006) 51.
[16] Y. Guan, Y. Liu, W. Wu, K. Sun, Y. Li, P. Ying, Z. Feng, C. Li, Langmuir 21 (2005) 3877.
[17] C.M. Yang, H.A. Lin, B. Zibrowius, B. Spliethoff, F. Schüth, S.C. Liou, M.W. Chu, C.H. Chen, Chem. Mater. 19 (2007) 3205.
[18] Y. Wang, C. Bryan, H. Xu, P. Pohl, Y. Yang, C.J. Brinker, J. Colloid Interf. Sci. 254 (2002) 23.
[19] H. Wang, Q. Liu, F. Gao, Q. Shi, Y. Yan, F. Zhang, S. Xie, B. Tu, D. Zhao, Adv. Funct. Mater. 15 (2005) 1377.
[20] Q.Z. Zhai, P. Wang, J. Iranian Chem. Soc. 5 (2008) 268.
[21] A. Charmot, Ph.D. Thesis, University of Poitiers, France, 2006.
[22] A.J. van Dillen, R.J.A.M. Terörde, D.J. Lensveld, J.W. Geus, K.P. de Jong, J. Catal. 216 (2003) 257.
[23] S. Valange, A. Charmot, J. Barrault, A. Louati, Z. Gabelica, Stud. Surf. Sci. Catal. 170A (2007) 531.
[24] Z. Gabelica, A. Charmot, R. Vataj, R. Soulimane, J. Barrault, S. Valange, J. Thermal Anal. Calorim. 95 (2009) 445.
[25] D. Zhao, J. Feng, Q. Huo, N. Melosh, G.H. Fredrickson, B.F. Chmelka, G.D. Stucky, Science 279 (1998) 548.
[26] Z. Gabelica, S. Valange, M. Shibata, H. Hotta, T. Suzuki, Micropor. Mesopor. Mater. 44–45 (2001) 645.
[27] A. Galarneau, H. Cambon, F. Di Renzo, R. Ryoo, M. Choi, F. Fajula, New J. Chem. 27 (2003) 73.
[28] D.B. Bukur, C. Sivaraj, Appl. Catal. A 231 (2002) 201.
[29] Á. Szegedi, G. Pál-Borbély, K. Lázár, React. Kinet. Catal. Lett. 74 (2001) 277.
[30] S. Valange, J. Barrault, A. Derouault, Z. Gabelica, Micropor. Mesopor. Mater. 44–45 (2001) 211.
[31] E. Brendle, A. Louati, Electroanalysis 12 (2000) 1147.
[32] C. Borges, M.F. Ribeiro, C. Henriques, J.P. Lourenço, D.M. Murphy, A. Louati, Z. Gabelica, J. Phys. Chem. B 108 (2004) 8344.